Distinct Microbes, Metabolites, and Ecologies Define the Microbiome in Deficient and Proficient Mismatch Repair Colorectal Cancers

Vanessa L. Hale[1,2,3,*], Patricio Jeraldo[2,3,*], Jun Chen[2,4], Michael Mundy[5], Janet Yao[2], Sambhawa Priya[6], Gary Keeney[7], Kelly Lyke[3], Jason Ridlon[8], Bryan A. White[8], Amy J. French[7], Stephen N. Thibodeau[7], Christian Diener[9], Osbaldo Resendis-Antonio[9,10], Jaime Gransee[11], Tumpa Dutta[11], Xuan-Mai Petterson[11], Ran Blekhman[6], Lisa Boardman[12], David Larson[13], Heidi Nelson[2,13], and Nicholas Chia[2,3,†].

[1]Department of Veterinary Preventive Medicine, The Ohio State University College of Veterinary Medicine, Columbus, OH, USA

[2]Microbiome Program, Center for Individualized Medicine, Mayo Clinic, Rochester, MN, USA

[3]Division of Surgical Research, Department of Surgery, Mayo Clinic, Rochester, MN, USA

[4]Department of Health Sciences Research, Mayo Clinic, Rochester, MN, USA

[5]Center for Individualized Medicine, Mayo Clinic, Rochester, MN, USA

[6]Department of Genetics, Cell Biology, and Development, University of Minnesota, Minneapolis, MN, USA

[7]Division of Laboratory Medicine and Pathology, Mayo Clinic, Rochester, MN, USA

[8]Carl R. Woese Institute for Genomic Biology, Department of Animal Sciences, Division of Nutritional Sciences, University of Illinois, Urbana-Champaign, IL, USA

[9]Human Systems Biology Laboratory, National Institute of Genomic Medicine, Mexico City, Mexico

[10]Coordinación de la Investigación Científica, Red de Apoyo a la Investigación, UNAM, Mexico City, Mexico

[11]Mayo Clinic Metabolomics Core Laboratory, Mayo Clinic, Rochester, MN, USA

[12]Division of Gastroenterology and Hepatology, Mayo Clinic, Rochester, MN, USA

[13]Division of Colon and Rectal Surgery, Department of Surgery, Mayo Clinic, Rochester, MN, USA

[*]These authors contributed equally to this work

[†]Corresponding author: chia.nicholas@mayo.edu

ABSTRACT [350 word limit: 326]

Background

The link between colorectal cancer (CRC) and the gut microbiome has been established, but the specific microbial species and their role in carcinogenesis remain controversial. Our understanding would be enhanced by better accounting for tumor subtype, microbial community interactions, metabolism, and ecology.

Methods

We collected paired colon tumor and normal–adjacent tissue and mucosa samples from 83 individuals who underwent partial or total colectomies for CRC. Mismatch repair (MMR) status was determined in each tumor sample and classified as either deficient MMR (dMMR) or proficient MMR (pMMR) tumor subtypes. Samples underwent 16S rRNA gene sequencing and a subset of samples from 50 individuals were submitted for targeted metabolomic analysis to quantify amino acids and short-chain fatty acids. A PERMANOVA was used to identify the biological variables that explained variance within the microbial communities. dMMR and pMMR microbial communities were then analyzed separately using a generalized linear mixed effects model that accounted for MMR status, sample location, intra–subject sample correlation, and read depth. Genome–scale metabolic models were then used to generate microbial interaction networks for dMMR and pMMR microbial communities. We assessed global network properties as well as the metabolic influence of each microbe within the dMMR and pMMR networks.

Results

We demonstrate distinct roles for microbes in dMMR and pMMR CRC. Sulfidogenic *Fusobacterium nucleatum* and hydrogen sulfide production were significantly enriched in dMMR CRC, but not pMMR CRC. We also surveyed the butyrate–producing microbial species, but did not find a significant difference in predicted or actual butyrate production between dMMR and pMMR microbial communities. Finally, we observed that dMMR microbial communities were predicted to be less stable than pMMR microbial communities. Community stability may play an important role in CRC development, progression, or immune activation within the respective MMR subtypes.

Conclusions

Integrating tumor biology and microbial ecology highlighted distinct microbial, metabolic, and ecological properties unique to dMMR and pMMR CRC. This approach could critically improve our ability to define, predict, prevent, and treat colorectal cancers.

Introduction

The gut microbiota has been linked to colorectal cancer (CRC) in many studies [1–7], and serves as a very promising target for diagnostic, prophylactic, and therapeutic applications. Yet, despite intense study, only a few microbial species—like *Fusobacterium* species—are consistently observed across studies [5–8], while many microbial associations appear to be cohort–specific. Meta–analyses have attempted to overcome the limited statistical power of smaller studies [9] but are limited by the strong biases introduced through varying collection, sequencing, and data processing methodologies [10–13]. Mechanistic studies in mouse models have identified strong causative links between specific microbes (e.g. *Fusobacterium nucleatum, Bacteroides fragilis*) and CRC development and progression [14–17], but these models have limited applicability in genetically diverse human populations. Capturing some of this genetic diversity, on the other hand, may improve our ability to discriminate tumor and normal microbial communities and more clearly define pathways to CRC.

There are multiple subtypes of CRC: one broad categorization is based on mismatch repair (MMR) status. MMR status divides CRCs into two groups: deficient mismatch repair (dMMR) and proficient mismatch repair (pMMR)[18]. In general, dMMR CRCs are hypermethylated, hypermutated, and associated with BRAF V600E mutations; whereas, pMMR CRCs are generally microsatellite stable (MSS) and associated with KRAS[19]. These distinct molecular subtypes of CRC are also borne out by evidence that dMMR is specifically associated with the β-catenin signaling pathway[20]. Clinically, MMR status is associated with patient prognosis, and age, as well as tumor location and stage: Specifically, dMMR CRCs have a better prognosis and occur more often on the right side of the colon in older patients with early stage CRC[18].

Finally, dMMR and pMMR CRC not only have different endpoints, but may also have different paths to tumorigenesis[21] as supported emerging evidence that dMMR CRC arises from sessile serrated adenomas [22] as opposed to the more classic tubular adenoma associated with pMMR CRC [22].

The distinct phenotype of dMMR CRC suggests that host—and possibly also microbial—dynamics are greatly altered in association with deficient mismatch repair. However few CRC microbiome studies account for MMR status [23, 24] or microbial dynamics [2], and no studies, to our knowledge, have assessed both MMR status and microbial community dynamics.

Here, we undertook a new approach in a study involving 83 patients who underwent partial or total colectomy for CRC. From each patient, we collected colon tissue and mucosal samples at tumor and normal–adjacent sites. MMR status was extracted from patient records or determined by testing formalin–fixed paraffin embedded tumor tissue for the expression of four MMR proteins (MLH1, MSH2, MSH6, PMS2). Patient tumors were characterized as either deficient (dMMR) or proficient (pMMR) mismatch repair. Microbial composition was assessed via 16S rRNA gene sequencing. A subset of colon tissue samples additionally underwent metabolomic analysis to quantify amino acids and short-chain fatty acids (SCFAs). A portion of these data was published previously [2] in a study that highlighted the value of integrating *in silico* genome–scale metabolic model predictions and *in vivo* experimental metabolomic data.

From these data, we assessed the relative importance of MMR status compared to other biological factors reported to alter the microbiome[25]. MMR status was the strongest predictor

of microbial community variance in comparison to sample location (proximal/distal and on/off tumor), body mass index (BMI), age, and sex. Separate analyses of the dMMR and pMMR microbial communities revealed that many common CRC–associated microbial signatures[9, 26]—including *Fusobacterium nucleatum, Fusobacterium periodonticum,* and *Bacteroides fragilis*—were all enriched in dMMR but not pMMR tumors. Functional differences were examined using a combination of metabolomics and community metabolic modeling. Our results indicate greater predicted and actual hydrogen sulfide production in dMMR CRC as compared to pMMR CRC, but no significant differences in predicted or actual butyrate production. Finally, we approximated microbial ecology by modeling the metabolic interactions between microbes. Overall, the pMMR microbial network was predicted to be more stable (resistant to disturbances). Microbial community stability may play an important role in tumorigenesis, cancer progression, and immune activation [22, 27, 28], and only by examining predicted microbial community interactions were we able to capture this dynamic. Our work demonstrates distinct microbial, metabolic, and ecological attributes of dMMR and pMMR microbial communities, serving to further emphasize the importance of considering tumor biology and microbial interactions in studies of the CRC microbiome.

Methods

Human subject enrollment

This study was performed with the approval of the Mayo Clinic Institutional Review Board (IRB# 14-007237 and IRB# 622-00). Written informed consent was obtained from all individuals in the study. Adults (older than 18 years old) who were determined to be candidates

for colorectal cancer surgery were voluntarily enrolled at Mayo Clinic in Rochester, Minnesota. Exclusion criteria included chemotherapy or radiation in the 2 weeks leading up to enrollment. Total or partial colectomies were performed on every patient, and colon tissue and mucosal samples were collected from tumor and normal–adjacent sites. Sample location was defined as follows: "proximal" samples were derived from the cecum and ascending colon. "Distal" samples were derived from the transverse, descending, or sigmoid colon, or rectum. MMR status was determined in 83 patients: 25 had dMMR CRC and 58 had pMMR CRC (**Table 1**). We used univariable logistic regression (R v3.1.2) to compare demographic (age, sex, BMI, smoking history) and disease features (tumor location and stage) between dMMR and pMMR groups.

Table 1. Demographic and disease features of individuals identified as having dMMR or pMMR CRC.

	dMMR	pMMR	p-value
Sex, n (%)			
Male	10 (40)	34 (59)	0.122
Female	15 (60)	24 (41)	
Age , yr			
Mean (SD)	74 (18)	63 (13)	0.002
Range	23-95	33-90	
BMI (SD)	27 (5)	29 (8)	0.273
Smoke ever?			
Yes	13 (52)	28 (48)	0.982
No	12 (48)	30 (52)	
Tumor location, n (%)			p < 0.0001
Proximal Colon	18 (72)	14 (24)	between
Distal Colon	7 (28)	43 (74)	proximal
Both	0	1 (3)	and distal
Stage, n (%)			0.0007
Early (1-2)	18 (72)	22 (38)	between
Late (3-4)	4 16)	33 (57)	early and
Stage unknown	3 (12)	3 (5)	late

150 **MMR status determination**

151 Mismatch repair (MMR) pathway and microsatellite instability (MSI) test results were extracted
152 from patient records if available. For patients without MMR test results, banked formalin–fixed
153 paraffin–embedded colon tumor tissue blocks were submitted to the Mayo Clinic Pathology
154 Resource Core for sectioning into 10 micron–thick slices. Slices were then submitted to the
155 Mayo Clinic Molecular Genetics Laboratory for immunohistochemistry staining of MMR
156 proteins (MLH1, PMS2, MSH2, MSH6).

157

158 **16S DNA extraction, sequencing, and sequence processing**

159 DNA extraction[26] and library preparation on colon tissue (tumor and normal–adjacent), and
160 mucosa were performed as described previously in the Mayo Clinic Microbiome Laboratory [2].
161 Samples were submitted for 16S rRNA gene sequencing (V3–V5 region) at the Mayo
162 Clinic Medical Genomics Facility (Illumina MiSeq, 2□×□300, 600 cycles, Illumina Inc.).
163 Sequencing yielded a total of 41,400,384 reads with a median of 70,208 reads per sample. Reads
164 were processed using DADA2 v1.6 to obtain error–corrected amplicon sequence variant
165 representatives—analogous to operational taxonomic units with single-nucleotide resolution
166 (sOTUs) [29]. sOTUs were annotated with genus–level taxonomy using the RDP Naïve
167 Bayesian Classifier[30] as implemented in DADA2 and, if possible, to species level using
168 DADA2, both against the SILVA 16S database, v132[31]. sOTUs annotated as Chloroplast and
169 Mitochondria were removed. Resulting sOTUs were filtered for possible non-specific
170 amplification using SortMeRNA v2.0[32] and Infernal v1.1.2[33]. sOTUs with fewer than 10
171 reads across all samples were excluded. Multiple sequence alignment of the sOTUs was

performed using Infernal v1.1.2[33], and an approximate Maximum Likelihood phylogeny was calculated using FastTree v2.1.9[34]. Raw sequencing data can be found at the NCBI Sequence Read Archive with primary BioProject accession number PRJNA445346 (**Additional File 2** - sOTU table, **3** - sOTU taxonomy, **4**- sOTU fasta file).

Statistical analyses of 16S rRNA microbial community data

An unweighted UniFrac distance matrix [35] based on the microbial communities in all samples was generated using the phyloseq[36] package v1.22.3. A permutational multivariate analysis of variance (PERMANOVA) was then performed on the distance matrix to assess the effects of MMR status and sample location (proximal/distal and on/off tumor) on variance between microbial communities. The PERMANOVA additionally accounted for subject age, sex, BMI, and sample type (mucosa versus colon tissue) and was performed using the adonis2 function in the vegan[37] package v2.5-1, with 999 bootstrap iterations.

A Generalized Linear Mixed Model (GLMM)[38] was calculated for each sOTU to estimate its abundance (read counts) in relation to predictors that included MMR status and sample location (proximal/distal and on/off tumor). Models were corrected for subject intervariability, specimen type (mucosal vs tissue biopsy), and sequencing read depth, allowing for interactions. We used the package glmmTMB[39] v0.1.4 to estimate the abundance of each microbe under a zero–inflated Poisson distribution. For each predictor, sOTUs were excluded where the method did not converge or the Akaike Information Criterion (AIC) for model quality was not defined. Multiple hypothesis correction was calculated using the Benjamini–Hochberg procedure.

194

195 **Validation of differentially abundant microbes using an independent cohort**

196 To validate the differentially abundant microbes associated with dMMR status, we investigated
197 data from a recent study that included microbiome profiling in tumor and matched normal tissue
198 samples in 44 CRC patients [1]. We categorized MMR status based on microsatellite instability
199 (MSI) / microsatellite stable (MSS) status (MSI was categorized as dMMR; MSS was
200 categorized as pMMR) or downregulation of any of the 4 MMR genes (MLH1, MSH2, MSH6
201 and PMS2) as assessed using RNA-Seq in the same samples. A cutoff (log2(normal/tumor) > =
202 1) was used to call a gene as downregulated in tumor. Altogether, we identified 9/44 patients as
203 dMMR and the remaining 35/44 as pMMR. Using 16S rRNA gene microbiome characterization
204 for these samples (as described in detail in [1]) we identified sOTUs associated with dMMR
205 tumor/normal and pMMR tumor/normal conditions. We first filtered rare sOTUs, only
206 preserving sOTUs found in at least 50% of our samples, and then performed differential
207 abundance analysis using phyloseq[36] (which uses DESeq2 to build negative binomial
208 generalized linear models). We used the Benjamini–Hochberg method to control for the false
209 discovery rate (FDR).

210

211 **Real-time PCR for the *Bacteroides fragilis* toxin gene**

212 Real-time PCR was performed as described previously [2] to test colon tissue and mucosal
213 samples for the presence of the *Bacteroides fragilis* toxin (BFT) genes in 22 dMMR individuals
214 and 53 pMMR individuals. Primers included: BFT-F (5'-
215 GGATAAGCGTACTAAAATACAGCTGGAT-3'), BFT-R (5'-

CTGCGAACTCATCTCCCAGTATAAA-3'), and the probe (5'-FAM-CAGACGGACATTCTC-NFQ-MGB-3')[14].

Modeling microbial hydrogen sulfide production

We predicted hydrogen sulfide production within dMMR and pMMR tumor and normal–associated microbial communities as described previously[2]. Briefly, we aligned 16S rRNA gene sequences for dMMR tumor and normal samples (colon tissue and mucosa) and pMMR tumor and normal samples against complete genomes in PATRIC and then generated genome–scale metabolic models of each microbe (**Additional File 1: Table S1**). Genome–scale metabolic models use gene annotations from a microbial genome to predict the metabolic inputs and outputs of that microbe. To predict how a microbe might interact within a community, we used MICOM, an open-source platform to assess microbial metabolic community interactions (https://github.com/resendislab/micom). Specifically, we evaluated hydrogen sulfide flux as a measure of hydrogen sulfide production within each microbial community.

Metabolomics sample preparation and analysis

Colon tissue and mucosa samples were prepared and run as described previously[2]. In brief, UPLC–MS was used to quantify amino acid proxies for hydrogen sulfide including serine, homoserine, lanthionine, L-cystathionine, and D-cystathionine. GC–MS was used to quantify SCFAs including acetate, propionate, isobutyrate, butyrate, isovaleric acid, valeric acid, isocaproic acid, and hexanoate[2]. Significance testing was performed using Kruskal–Wallis and Dunn's *post hoc* tests in R v3.4.1

238

239 **Microbial influence network**

240 To select sOTUs for the Microbial Influence Networks (MINs), we used GLMM results to
241 choose tumor and normal–associated microbes in dMMR and pMMR samples with a linear
242 effect size greater than 0.25, regardless of statistical significance. Effect size captures biological
243 impact potential while significance measures certainty. In this case, we wanted to assess the
244 metabolic influence (i.e., biological impact) of microbes in relation to their respective microbial
245 communities; as such, it was more appropriate to filter by effect size. For each sOTU, the 16S
246 rRNA gene consensus sequence was aligned against complete genome in the PATRIC system
247 using VSEARCH v2.7.1, with a minimum nucleotide identity of 90%. When this procedure
248 generated multiple top hits, we selected a genome, in order, to the most complete genome (fewer
249 contigs), a type strain, a strain with a binomial name, and the closest match to the 16S taxonomy
250 (when possible). For each genome, we then reconstructed and downloaded its corresponding
251 genome–scale metabolic model using the PATRIC service. When sOTUs mapped to the same
252 model, we used that model only once, effectively merging those sOTUs in further analysis, with
253 an exception for when two sOTUs were associated with opposite conditions (i.e., tumor and
254 normal–adjacent samples), in which case we discarded that model from further consideration.
255 The decision to discard was also based on the observation that low identity hits or sOTUs with
256 taxonomy not sufficiently resolved were typically involved in these few cases.

257

258 After obtaining the genome–scale metabolic models (GEMs), we calculated “growth” on
259 complete media with no oxygen. This was done by calculating optimal metabolic reaction fluxes

using a Flux Balance Analysis[40], in which "growth" is the calculated flux of the reaction defining biomass for a microbe. We did this using a tool for assessing microbial metabolic interactions (MMinte) which evaluates the growth of microbes alone and when paired with another microbe [41]. Once single and paired growth values were calculated using the objective function given by MMinte[41], these values were then used to calculate the influence score. The interaction score, α_{ij}, for each species, m, with a different species x was calculated as

$$\alpha_{xm} = g(m|x) - g(x)\# \quad (1)$$

where $g(x)$ was the growth rate of x alone, and $g(m|x)$ was the growth rate of x in a community composed of both x and m. Based on these scores, we then calculated the unweighted metabolic influence of each individual microbial model on the other microbes in the community as the sum of the absolute value of the difference in growth rates when paired with species m,

$$G_m = \sum_j |\alpha_{jm}| = \sum_j |g(m|j) - g(j)| \#(2)$$

This scoring closely follows the spirit of the scoring from the global interaction modeling in Sung *et al*.[42] with use of actual growth rates instead of summing over shared transporters. Metabolic modeling based on flux balance analysis, as described here, provides a means to calculate a rate in the change of growth, as normalized per unit mass, allowing us to take a simple sum in order to calculate influence under anaerobic conditions.

The percentage of negative interactions was calculated by counting the number of negative interactions over the number of total interactions in each microbial influence network (MIN).

Statistical significance was based on the probability of getting equivalent results in dMMR and pMMR networks using the measured distributions of negative and positive interactions in each network and a scheme of random selection with replacement.

Finally, the resulting MIN[42] was visualized using Cytoscape v3.6.1[43] with node and edge properties weighed according to influence score and influence, respectively. Initial visualization in Cytoscape was generated using the "Edge–weighted spring–embedded layout" with the parameters modified to avoid node collisions according to what worked best in each of the two cases. Node sizes and edge weights were likewise set according to the maximum and minimum values in dMMR and pMMR networks separately. Interactions below 10 in the case of dMMR and below 5 in the case of pMMR were excluded from the spring force layout computation in order to achieve better readability of the final network figure. Unconnected nodes that had no influence were not included in the visualization.

Predicting butyrate production

After we identified the most influential microbes in the dMMR and pMMR MINs, we then assessed the butyrate–producing potential of these microbes. We used the previously selected genome sequences for these microbes and queried the PATRIC service [44] for the presence of the following genes: butyrate kinase (EC 2.7.2.7) or acetate CoA-transferase (EC 2.8.3.8). These genes serve as markers for butyrate production pathways [45]. The presence of either gene was considered sufficient to establish that a bacterium was capable of producing butyrate.

Results

dMMR tumors associated with older age and early stage, proximal tumors

A total of 25 individuals with dMMR CRC and 58 individuals with pMMR CRC were involved in this study. Individuals with dMMR CRC were significantly older than individuals with pMMR CRC and significantly more likely to have an early stage, proximal tumor (**Table 1**). As such, we included age and sample location (proximal/distal and on/off tumor) as covariates in subsequent analyses.

Tumor MMR status strongly predicts variance between microbial communities

To assess factors that contributed to variance in the microbial community data, we performed a PERMANOVA analysis on unweighted UniFrac distances between microbial communities in each sample. We included MMR status, sample location (proximal/distal, on/off tumor), age, sex, BMI and sample type (colon tissue vs. mucosa) as potential predictors of the variance. Remarkably, we found that MMR status explained more of the variance than any of the other 6 variables (**Additional File 1: Table S2**) even when MMR status was included as the last variable in the model (**Table 2**).

Table 2. Factors contributing to variance between microbial communities. MMR status was included as the last variable in this model and accounts for the greatest percent variance (PERMANOVA; see also **Additional File 1: Table S2**).

Factors	% Variation	R^2	F	Pr(>F)
BMI	1.53	0.013438	8.028927	1.00E-04
Age	1.18	0.010349	6.183355	1.00E-04
Sex	1.77	0.015529	9.278172	1.00E-04

Sample type	1.92	0.016848	10.06614	1.00E-04
Sample location - proximal / distal	2.07	0.018191	10.86858	1.00E-04
Sample location - on/off tumor	1.26	0.011050	6.60250	1.00E-04
MMR status	2.11	0.018527	11.06941	1.00E-04
Sample location – proximal / distal: Sample location - on/off tumor	0.21	0.001802	1.076725	0.3185
Sample location – proximal / distal:MMR status	1.10	0.009634	5.7563	1.00E-04
Sample location - on/off tumor:MMR status	0.29	0.002572	1.537264	0.0411
Sample location – proximal / distal:Sample location - on/off tumor:MMR status	0.19	0.001670	0.99816721	0.4245
Residual	100.21	0.880385	NA	NA
Total	113.82	1	NA	NA

Distinct microbial communities associated with pMMR and dMMR tumors

Given the importance of MMR status to microbial community variance, we opted to assess microbial abundances in tumor and normal samples for each MMR subtype independently. We identified multiple differentially abundant sOTUs in dMMR and pMMR tumor samples as compared to normal–adjacent samples using a generalized linear mixed model (GLMM) that accounted for sample location, sample type, and intrasubject sample correlation (**Fig. 2**; **Additional File 1: Figure S1** (Venn diagram showing counts of microbes in each group**), Table S3** (table of microbes enriched in dMMR), **Table S4** (table of microbes enriched in pMMR). Several major butyrate producers were identified in dMMR and pMMR tumor and normal samples. Only one microbe—*Dorea longicatena*—was significantly enriched in both dMMR and pMMR tumor samples. Four microbes had opposite associations with tumor or normal samples depending on MMR status: *Faecalibacterium prausnitzii* A2-165 and *Blautia* sp. Marseille-

P2398 were significantly enriched in pMMR tumor and dMMR normal samples; *Coprococcus comes* ATCC 27758 and *Bacteroides massiliensis* B84634 were significantly enriched in dMMR tumor and pMMR normal samples. Notably, *Fusobacterium periodonticum, F. nucleatum,* and *Bacteroides fragilis*—microbes commonly associated with CRC[5, 14, 46–49]—were among the top most differentially abundant microbes in dMMR tumor samples but were not found to be differentially abundant in pMMR tumor samples.

To validate these results, we used publicly available data from tumor and matched normal samples from 44 CRC patients[1]. Our validation analysis showed several overlapping associations of microbial genomes with respect to dMMR and pMMR in tumor and matched normal samples (**Additional File 1: Table S5, S6)**. dMMR tumors were found enriched for *Bacteroides fragilis* (p=0.02, FDR p=0.37) and *Fusobacterium* (p=0.03, FDR p=0.37) while dMMR normal samples were enriched for *Dorea* (p=0.03, FDR p=0.37) and an Erysipelotrichaceae bacterium (p=0.007, FDR p=0.31) (**Additional File 1: Figure S2**). Even though these associations were not statistically significant after correcting for FDR, their trend of association overlaps with the results from the present study. Differentially abundant sOTUs between pMMR tumors versus normal included Ruminococcaceae, *Faecalibacterium prausnitzii* and *Bacteroides caccae*, which were also differentially abundant in the present study.

As *B. fragilis* was significantly enriched in dMMR tumors, and there are well-established links between toxigenic *B. fragilis* and colorectal cancer [14, 46, 50], we next looked for the presence of the *B. fragilis* toxin (BFT) gene in dMMR and pMMR tissue and mucosa samples. Of the 22

355 individuals with dMMR CRC, only samples from 1 was BFT positive (5%); of 53 individuals
356 with pMMR CRC, samples from 5 were BFT positive (9.4%). There was no significant
357 difference in BFT presence between individuals with dMMR or pMMR CRC (Chi-squared, p =
358 0.477).

359

360 **Microbial hydrogen sulfide production enriched in the dMMR CRC tumors**

361 As sulfidogenic *F. nucleatum* and *F. periodonticum* were also significantly enriched in dMMR
362 tumor samples, we decided to assess potential hydrogen sulfide production across groups
363 (dMMR/pMMR, tumor/normal) by modeling hydrogen sulfide flux. We used microbial
364 community metabolic models to predict hydrogen sulfide flux within each microbial community
365 (dMMR tumor and normal, pMMR tumor and normal). The models produced a non–significant
366 trend towards increased hydrogen sulfide flux in dMMR tumor samples (**Fig. 3a**). To get a more
367 concrete measure of hydrogen sulfide production, we ran targeted metabolomics to quantify
368 amino acid proxies (serine, homoserine, lanthionine, L-cystathionine, D-cystathionine) for
369 hydrogen sulfide in dMMR and pMMR tumor and normal tissue samples (**Fig. 3b**). We observed
370 a significant increase in lanthionine in dMMR tumor tissue over dMMR or pMMR normal tissue
371 and pMMR tumor. Homoserine and L-Cystathionine were also significantly increased in both
372 dMMR and pMMR tumor tissue as compared to normal–adjacent tissue. The metabolomics
373 results suggest increased hydrogen sulfide production in tumor tissue—particularly in dMMR
374 tumor tissue.

375

376 **pMMR microbial community predicted to be more stable and to suppress *F. nucleatum***

To further assess the potential metabolic interactions between tumor and normal–adjacent microbes in relation to MMR status, we constructed two metabolic influence networks (MIN; **Fig. 1**)[42]. The MIN highlights each microbe's predicted influence and interactions (growth enhancing or suppressing) in relation to other microbes in the community. We also evaluated an indirect measure of ecological stability[51] based on the percentage of predicted positive and negative interactions present within a given microbial community. Notably, the more negative interactions present within a community, the more stable that community is predicted to be[51]. The dMMR microbial community exhibited 21.1% negative interactions while the pMMR microbial community exhibited significantly more (47.6%, binomial test, $p<0.0001$), suggesting that the pMMR community is more stable.

Also of note in relation to the dMMR MIN, *F. nucleatum* and *F. periodonticum* exhibit no metabolic interactions with the other microbes in the network and therefore were not included in the network visualization. In contrast, in the pMMR MIN, *F. nucleatum*—one of the most influential microbes—was uniformly suppressed by 34 out of 44 other pMMR–associated microbes, with zero positive interactions.

Highly influential microbes include many butyrate producers

Within the MINs, microbes that exhibit many or strong interactions with other microbes—either influencing or being influenced by—are classified as influential microbes. To examine the most influential microbes within each MIN, we identified all microbes with an influence score of 0.5 standard deviations above the mean for dMMR and pMMR microbes, respectively (**Tables 3** –

399 dMMR**, 4 –** pMMR). Characterization of the most influential microbes revealed that many of

400 these microbes are butyrate producers.

401 **Table 3**. List of basic properties for the most influential microbes in the dMMR MIN.

dMMR–associated microbes	Influence score	tumor/normal	PATRIC genome ID	butyrate producer?	relevant citations
Pseudomonas aeruginosa	1732.80	**tumor**	287.2537		[52]
***Faecalibacterium prausnitzii* A2-165**	1615.38	normal	411483.3	x	[53]
***Ruminococcus torques* L2-14**	1516.19	normal	657313.3		[54]
***Escherichia coli* K-12**	1452.80	normal	511145.12		[55]
Flavonifractor plautii	1431.48	normal	292800.4		[56]
Eubacterium ramulus	1407.40	normal	39490.3		[56]
Dorea formicigenerans	1407.33	normal	411461.4		[57]
Roseburia intestinalis	1401.32	**tumor**	657315.3	x	[53]
***Faecalibacterium prausnitzii* SL3/3**	1395.95	normal	657322.3	x	[53]
Streptococcus salivarius	1395.74	normal	1304.182		[58]
***Ruminococcus torques* ATCC 27756**	1393.15	normal	411460.6		[54]
Clostridium symbiosum	1382.77	**tumor**	1512.4	x	[59]
Pelotomaculum thermopropionicum	1376.65	normal	370438.4		[60]
Clostridium clostridioforme	1368.34	**tumor**	999403.4	x	[61]
***Coprobacillus* sp. 8_1_38FAA**	1363.69	normal	450746.3	x	[62]

402

403

404

405

406

407

408

409

410

411

412

413

414 **Table 4**. List of basic properties for the most influential microbes in the pMMR MIN.

pMMR–associated microbes	influence	tumor/normal	PATRIC genome ID	butyrate producer?	relevant citations
Firmicutes bacterium ASF500	1001.50	**tumor**	1378168.3		[63]
Ruminococcus sp. A254.MGS-254	951.21	**tumor**	1637499.3		[64]
Bacteroides massiliensis B84634 =	833.96	normal	1121098.3		[65]

Timone 84634 = DSM 17679 = JCM 13223 [PRJNA201686]					
Fusobacterium nucleatum CTI-5	832.56	**tumor**	1316586.3		[47, 66]
Prevotella copri DSM 18205	827.75	**tumor**	537011.5		[57]
Dorea longicatena	821.96	**tumor**	88431.7		[57]
***Clostridium bolteae* 90A9**	797.92	**tumor**	997894.4	x	[61]
Anaerotruncus colihominis DSM 17241	780.61	normal	445972.6	x	[67]
Coprococcus comes ATCC 27758	779.84	normal	470146.3	x	[68]
Campylobacter gracilis strain ATCC 33236	766.50	**tumor**	824.5		[69]

Butyrate production did not differ between dMMR and pMMR microbial communities

Given the predicted influence and differential abundance of butyrate–producing microbes in dMMR and pMMR, we decided to compare the butyrate–producing potential of the most influential tumor–associated microbes in dMMR and pMMR MINs by searching for genes involved in butyrate production within the functional annotation of these genomes in PATRIC. There were no significant differences in butyrate production–associated genes between dMMR and pMMR tumor–associated microbes (**Table 5;** Wilcoxon rank-sum test, $p>0.05$). To more fully assess community–wide butyrate production, we performed targeted metabolomics to quantify SCFA concentrations in tumor and normal–adjacent colon tissue. With the exception of isocaproic acid, which was significantly increased in dMMR tumor tissue, there were no significant differences in SCFA concentrations—including butyrate—between dMMR tumor and normal–adjacent or pMMR tumor and normal–adjacent tissue samples (**Fig. 4**).

Table 5. Percent of the most influential tumor–associated microbes in dMMR and pMMR CRC that contain a butyrate–producing pathway, as predicted by the presence of genes involved in butyrate production.

Gene annotation	EC number	dMMR	pMMR
Acetate CoA-transferase	2.8.3.8	14.9%	13.8%
Butyrate kinase	2.7.2.7	27.7%	31.0%

431

432 To further explore how the dMMR MIN could have multiple strongly influential butyrate–
433 producing microbes but no increase in butyrate production, we examined the predicted
434 interactions (positive and negative) of the most influential butyrate producers in the dMMR MIN
435 network (identified in **Table 3**). We found that butyrate producers were targets of more negative
436 interactions (26% negative interactions) as compared to all negative interactions in the dMMR
437 MIN network (21% negative interactions), suggesting growth suppression of butyrate producers
438 in the dMMR community (binomial test, $p = 0.02$). In contrast, the most influential butyrate
439 producers in the pMMR MIN network (identified in **Table 4**) were not a target for increased
440 negative interactions (binomial test, $p = 0.08$). We repeated this analysis using all differentially
441 abundant major butyrate producers in dMMR and pMMR microbial communities (identified in
442 **Fig. 2**). We found that while all butyrate producers (in dMMR or pMMR microbial
443 communities) were more likely to be targets of negative interactions, this was more strongly
444 evident in the dMMR microbial community (dMMR binomial test: p=6E-13, pMMR binomial
445 test p=0.008).

446

447 **Discussion**

448 This study integrates tumor biology and microbial ecology in a novel and powerful approach to
449 understanding colorectal cancer. Our results indicate that MMR status is one of the strongest
450 predictors of microbial community variance; however, few studies [23, 24], to date, include

MMR status in microbial community analysis of colorectal cancer. Interestingly, we also identified several differentially abundant microbes associated with dMMR but not pMMR tumor samples including *F. nucleatum*, *F. periodonticum*, and *B. fragilis.* We further validated these findings in an independent cohort[1], which underscores the importance of including MMR status in future CRC microbiome studies. We additionally characterized the predicted and actual metabolic profiles of dMMR and pMMR individuals in relation to hydrogen sulfide and butyrate production, and we generated a network of predicted interactions within the dMMR and pMMR microbial communities.

Hydrogen sulfide has been reported to both promote and inhibit colorectal cancer [70–73]. To assess the role of hydrogen sulfide within our study, we looked for sulfidogenic bacteria, predicted hydrogen sulfide production using community metabolic models, and measured hydrogen sulfide concentrations through targeted metabolomics for amino acid proxies. We found two significantly enriched hydrogen sulfide–producing *Fusobacterium* species and significantly increased hydrogen sulfide concentrations in dMMR tumor samples. In the microbial influence network, both *Fusobacterium* species exhibited zero predicted interactions—positive or negative—with other microbes in the network. Together, this suggests that these *Fusobacterium* species grow abundantly and unchecked by other microbes, and have the potential to produce large quantities of hydrogen sulfide. In contrast, the *F. nucleatum* found in pMMR MIN was predicted to be the target of 34 (100%) negative interactions, suggesting that its growth and metabolic output (hydrogen sulfide) are highly suppressed in pMMR individuals.

These intriguing results leads us to speculate on the relationship between *Fusobacterium* species, hydrogen sulfide production and dMMR CRC. Notably, *Fusobacterium* species have previously been associated with hypermethylation of MLH1, MSI, BRAF mutations, and poorly differentiated tumors[4, 47]—all of which are characteristics of dMMR CRC[74]. Hydrogen sulfide—a cytotoxic, genotoxic gas—has also been associated with CRC[70, 71], although its role is somewhat controversial[72, 73]. A recent report indicates that colon cancer cells may respond to hydrogen sulfide in a bell–shaped dose–dependent manner: at high concentrations, hydrogen sulfide inhibits the proliferation of cancer cells, while at lower concentrations, hydrogen sulfide can stimulate the proliferation of cancer cells[73, 75]. In dMMR, if high levels of hydrogen sulfide (and hydrogen sulfide producers) inhibit cancer proliferation, then we would expect individuals with dMMR to present with earlier stage cancer—which is indeed the case in our cohort and other reported cohorts [65]. dMMR CRC has also been associated with lower recurrence rates and a better prognosis[74]. In opposition to these findings are studies showing that *F. nucleatum* can potentiate tumorigenesis and that *F. nucleatum*–associated CRCs have a worse prognosis [4, 5].

Besides *Fusobacterium*, *Bacteroides fragilis* was also found to be significantly enriched in dMMR tumor samples. Toxigenic *B. fragilis* has well–established and causative links to inflammation, and CRC[50, 76], and inflammation has been linked to hypermethylation[77]. As such, we tested dMMR and pMMR tissue and mucosa samples for the presence of the *B. fragilis* toxin (BFT) gene but did not find a significant difference in the presence of the BFT gene between dMMR and pMMR individuals. Given these results, it is unclear what the significance of increased *B. fragilis* is in the dMMR tumor samples.

Butyrate has been another subject of intense investigation in relation to gut health and CRC[54, 57]. Conflicting work in murine models indicates that butyrate can act to repress or to accelerate polyp and tumor formation—resulting in the so–called butyrate paradox[78]. Recently, a dMMR CRC mouse model showed that microbially–produced butyrate accelerated tumorigenesis[24], indicating that the source of this paradox may have to do with the genetic model of CRC being used and that butyrate may therefore have different, even opposite, roles in different CRC subtypes. It was therefore intriguing that more butyrate producers were identified as highly influential in the dMMR MIN as compared to pMMR MIN. However, neither predicted (functional annotation) nor actual (metabolomic data) butyrate production differed significantly between dMMR and pMMR samples or tumor and normal samples in the metabolomic profile. One potential reason for this lack of difference surfaced when we examined the number of negative interactions targeted at butyrate producers in the dMMR and pMMR MINs. dMMR butyrate producers had a significantly higher probability of negative interactions as compared to pMMR butyrate producers. This suggests that, though present, these butyrate producers are being suppressed in dMMR microbial communities.

Negative interactions were also predicted to be significantly increased in the pMMR microbial community as a whole versus the dMMR microbial community. Negative interactions, implying competition, are an ecological hallmark of a stable community[51], which is both resistant and resilient to disturbance. We speculate that a less stable microbial community in dMMR individuals could mean constant community shifts and disturbances—resulting in increased

518 immune activation. The dMMR tumor phenotype is associated with increased immune
519 response[74], which may play a role in inhibiting cancer cell proliferation of dMMR tumors.

520

521 Overall, our study demonstrates the importance and value in considering tumor biology (MMR
522 status) and ecological interactions when evaluating microbial community data. Our work is
523 primarily descriptive and incorporates host clinical features, microbiome, metabolome, and
524 modeling data. While we make speculations based on these data, future prospective and
525 mechanistic studies are needed to test these ideas. We also recognize that selecting sequenced
526 genomes available in the database to represent 16S rRNA sOTUs cannot fully replace
527 metagenomic sequencing given well–known strain-to-strain variation in gene content. However,
528 these variations between strains are often largely in secondary metabolite pathways, rather than
529 core metabolic function, which is the main target of our modeling analysis.

530

531 Another limitation of this study is our inability to attribute a source to metabolomic data. While
532 butyrate is a microbial fermentation product, hydrogen sulfide and its amino acid proxies can be
533 produced by both humans and bacteria. Thus, the enriched hydrogen sulfide we detect in dMMR
534 tumor samples could potentially be attributed to increased hydrogen sulfide production within
535 tumor tissue, and indeed, this has been reported[73]. If this was the solely case here however, we
536 might expect to see similar increases in hydrogen sulfide in pMMR tumors—most of which are
537 later in stage than dMMR tumors. We did not see this, suggesting that it is feasible that the
538 increased hydrogen sulfide production in dMMR tumors is coming from an exogenous
539 (microbial) source. Notably, microbially produced hydrogen sulfide can be generated from

multiple pathways including the respiration of dietary taurine and sulfate as well as the degradation of sulfomucins. The amino acid proxies we use to assess hydrogen sulfide production only capture some, but not all of these potential pathways, so we may have underestimated hydrogen sulfide production.

Finally, the field of genome–scale metabolic modeling has only recently encompassed tools for community metabolic analyses[79], and many of the tools[41, 42, 80] are sensitive to the underlying quality of the metabolic models[44, 81]. Models vary greatly depending on the presence and accuracy genome annotations which will generally improve over time. Future work aimed at understanding and verifying microbial dynamics in relation to MMR status or other CRC subtypes could dramatically improve our ability to define, predict, prevent, and treat colorectal cancers.

Conclusions

This study provides a novel framework in which to examine colorectal cancer:

1. Host–microbe interactions: Tumor MMR status strongly predicted microbial community variance and was associated with distinct microbial, metabolic, and interaction profiles. Our approach incorporating tumor MMR status, microbiome, metabolome and modeling data allowed us unique insights into the role of hydrogen sulfide and hydrogen sulfide producers within the dMMR microbial community. Tumor biology (e.g. MMR status) and microbial ecology are inextricably linked, and it is critical that future studies account for both in order to understand and more precisely classify the many pathways to CRC.

2. Microbe–microbe interactions: Microbial influence networks provided *in silico* predictions of community stability and microbial interactions that aligned with *in vivo* metabolomics data: Suppression of sulfidogenic *F. nucleatum* and significantly lower hydrogen sulfide production in pMMR, and suppression of butyrate–producing bacteria in dMMR—which may explain the lack of difference in butyrate production between dMMR and pMMR samples. The validation of *in silico* data with *in vivo* tests provides support for a future of precision medicine tools that can accurately predict disease and the potential effects of prophylactic or therapeutic interventions on the microbiome. Microbes act within communities, and understanding and predicting these interactions will be key to developing targeted mechanisms to help prevent or treat colorectal cancer.

Acknowledgements

We would first like to thank the patients who volunteered for this study. We also thank the many other individuals who made this work possible including members of the Mayo Clinic Microbiome Laboratory, study coordinators, students, colorectal surgeons, program directors, and pathology assistants. We also specially acknowledge Donna Felmlee Devine and Caitlin Foss-Baumgard for their assistance with patient records in relation to this study. Finally, we gratefully acknowledge the following funding sources: NIH (R01CA179243; N.C. and V.L.H. and R01CA170357; L.B.), the Mayo Clinic Center for Cell Signaling in Gastroenterology (NIDDK P30DK084567), the Mayo Clinic Metabolomics Resource Core Pilot and Feasibility Award (U24DK100469), the Fred C. Andersen Foundation (H.N. and N.C.), the Mayo Clinic Center for Individualized Medicine, The Randy Shaver Cancer Research and Community Fund (R.B.) the Minnesota Partnership for Biotechnology and Medical Genomics (R.B.), The Alfred

P. Sloan Foundation (R.B.) O.R.A thanks the financial support coming from the National Institute of Genomic Medicine (INMEGEN) to develop the computational tool used for the microbiome analysis (MICOM).

Figure Legends

Fig. 1 Microbial influence networks for a) dMMR and b) pMMR microbial communities. Node size indicates a microbe's metabolic influence over other microbes. Edges are directional and weighted and indicate how one microbe affects the growth rate of another: grey edges indicate a positive interaction, i.e., predicted increase in growth when paired, while red edges indicate a negative interaction or a predicted suppression in growth when paired.

Fig. 2 Microbes identified as differentially abundant in tumor as compared to normal samples (tissue and mucosa) from individuals with dMMR or pMMR CRC. Microbes are listed in order of significance from greatest to least. Microbes in bold font are enriched in both dMMR and pMMR samples. For example, *Coprococcus comes* ATCC 27758 is significantly enriched in dMMR tumor samples and pMMR normal samples. (GLMM, all microbes listed have a Benjamini–Hochberg p-value<0.05.)

Fig. 3 a) Hydrogen sulfide flux predicted based on community metabolic modeling. b) Amino acid proxies for hydrogen sulfide were quantified using UPLC–MS on dMMR and pMMR tumor and normal–adjacent colon tissue samples (Kruskal–Wallis followed by Dunn's Test for *post hoc* comparisons: *p <0.05; **p<0.0005, ***p<0.0005, ****p<0.00005).

Fig. 4 SCFAs in dMMR and pMMR tumor and normal–adjacent colon tissue samples (Kruskal–Wallis followed by Dunn's Test for *post hoc* comparisons: *p <0.05).

607

608 **References**

609

610 1. Burns MB, Montassier E, Abrahante J, Priya S, Niccum DE, Khoruts A, et al. Colorectal
611 cancer mutational profiles correlate with defined microbial communities in the tumor
612 microenvironment. bioRxiv. 2018;:090795. doi:10.1101/090795.

613 2. Hale VL, Jeraldo P, Mundy M, Yao J, Keeney G, Scott N, et al. Synthesis of multi-omic data
614 and community metabolic models reveals insights into the role of hydrogen sulfide in colon
615 cancer. Methods. 2018. doi:10.1016/j.ymeth.2018.04.024.

616 3. Flemer B, Lynch DB, Brown JMR, Jeffery IB, Ryan FJ, Claesson MJ, et al. Tumour-
617 associated and non-tumour-associated microbiota in colorectal cancer. Gut. 2017;66:633–43.
618 doi:10.1136/gutjnl-2015-309595.

619 4. Mima K, Nishihara R, Qian ZR, Cao Y, Sukawa Y, Nowak JA, et al. Fusobacterium
620 nucleatum in colorectal carcinoma tissue and patient prognosis. Gut. 2016;65:1973–80.
621 doi:10.1136/gutjnl-2015-310101.

622 5. Kostic AD, Chun E, Robertson L, Glickman JN, Gallini CA, Michaud M, et al. Fusobacterium
623 nucleatum Potentiates Intestinal Tumorigenesis and Modulates the Tumor-Immune
624 Microenvironment. Cell Host Microbe. 2013;14:207–15.

625 6. Chen W, Liu F, Ling Z, Tong X, Xiang C. Human Intestinal Lumen and Mucosa-Associated
626 Microbiota in Patients with Colorectal Cancer. PLoS One. 2012;7:e39743.
627 doi:10.1371/journal.pone.0039743.

628 7. Flanagan L, Schmid J, Ebert M, Soucek P, Kunicka T, Liska V, et al. Fusobacterium
629 nucleatum associates with stages of colorectal neoplasia development, colorectal cancer and
630 disease outcome. Eur J Clin Microbiol Infect Dis. 2014.

631 8. Castellarin M, Warren RL, Freeman JD, Dreolini L, Krzywinski M, Strauss J, et al.
632 Fusobacterium nucleatum infection is prevalent in human colorectal carcinoma. Genome Res.
633 2012;22:299–306. doi:10.1101/gr.126516.111.

634 9. Drewes JL, White JR, Dejea CM, Fathi P, Iyadorai T, Vadivelu J, et al. High-resolution
635 bacterial 16S rRNA gene profile meta-analysis and biofilm status reveal common colorectal
636 cancer consortia. npj Biofilms Microbiomes. 2017;3.

637 10. Sinha R, Abu-Ali G, Vogtmann E, Fodor AA, Ren B, Amir A, et al. Assessment of variation
638 in microbial community amplicon sequencing by the Microbiome Quality Control (MBQC)
639 project consortium. Nat Biotechnol. 2017;35:1077.

640 11. Vogtmann E, Chen J, Amir A, Shi J, Abnet CC, Nelson H, et al. Comparison of collection
641 methods for fecal samples in microbiome Studies. Am J Epidemiol. 2017;185:115–23.

642 12. Sinha R, Chen J, Amir A, Vogtmann E, Shi J, Inman KS, et al. Collecting Fecal Samples for
643 Microbiome Analyses in Epidemiology Studies. Cancer Epidemiol Biomarkers Prev.
644 2016;25:407–16. doi:10.1158/1055-9965.EPI-15-0951.

645 13. Jeraldo P, Chia N, Goldenfeld N. On the suitability of short reads of 16S rRNA for
646 phylogeny-based analyses in environmental surveys. Environ Microbiol. 2011;13:3000–9.
647 doi:10.1111/j.1462-2920.2011.02577.x.

648 14. Housseau F, Sears CL. Enterotoxigenic Bacteroides fragilis (ETBF)-mediated colitis in Min

649 (Apc+/-) mice: A human commensal-based murine model of colon carcinogenesis. Cell Cycle.
650 2010;9:3–5.

651 15. Zackular JP, Baxter NT, Chen GY, Schloss PD. Manipulation of the Gut Microbiota Reveals
652 Role in Colon Tumorigenesis. mSphere. 2016;1:e00001-15. doi:10.1128/mSphere.00001-15.

653 16. Bishehsari F, Engen PA, Preite NZ, Tuncil YE, Naqib A, Shaikh M, et al. Dietary fiber
654 treatment corrects the composition of gut microbiota, promotes SCFA production, and
655 suppresses colon carcinogenesis. Genes (Basel). 2018;9.

656 17. Khazaie K, Zadeh M, Khan MW, Bere P, Gounari F, Dennis K, et al. Abating colon cancer
657 polyposis by Lactobacillus acidophilus deficient in lipoteichoic acid. Proc Natl Acad Sci.
658 2012;109:10462–7.

659 18. French AJ, Sargent DJ, Burgart LJ, Foster NR, Kabat BF, Goldberg R, et al. Prognostic
660 significance of defective mismatch repair and BRAF V600E in patients with colon cancer. Clin
661 Cancer Res. 2008;14:3408–15.

662 19. Guinney J, Dienstmann R, Wang X, De Reyniès A, Schlicker A, Soneson C, et al. The
663 consensus molecular subtypes of colorectal cancer. Nat Med. 2015;21:1350.

664 20. Mårtensson A, Oberg A, Jung A, Cederquist K, Stenling R, Palmqvist R. Beta-catenin
665 expression in relation to genetic instability and prognosis in colorectal cancer. Oncol Rep.
666 2007;17:447–52.

667 21. Morkel M, Riemer P, Bläker H, Sers C. Similar but different: distinct roles for KRAS and
668 BRAF oncogenes in colorectal cancer development and therapy resistance. Oncotarget.
669 2015;6:20785–800.

670 22. Sweetser S, Jones A, Smyrk TC, Sinicrope FA. Sessile Serrated Polyps are Precursors of
671 Colon Carcinomas With Deficient DNA Mismatch Repair. Clin Gastroenterol Hepatol.
672 2016;14:1056–9.

673 23. Purcell R V., Visnovska M, Biggs PJ, Schmeier S, Frizelle FA. Distinct gut microbiome
674 patterns associate with consensus molecular subtypes of colorectal cancer. Sci Rep.
675 2017;7:11590. doi:10.1038/s41598-017-11237-6.

676 24. Belcheva A, Irrazabal T, Robertson SJJ, Streutker C, Maughan H, Rubino S, et al. Gut
677 Microbial Metabolism Drives Transformation of Msh2-Deficient Colon Epithelial Cells. Cell.
678 2014;158:288–99. doi:10.1016/j.cell.2014.04.051.

679 25. Chen J, Ryu E, Hathcock M, Ballman K, Chia N, Olson JE, et al. Impact of demographics on
680 human gut microbial diversity in a US Midwest population. PeerJ. 2016;4:e1514.
681 doi:10.7717/peerj.1514.

682 26. Hale VL, Chen J, Johnson S, Harrington SC, Yab TC, Smyrk TC, et al. Shifts in the fecal
683 microbiota associated with adenomatous polyps. Cancer Epidemiol Prev Biomarkers.
684 2017;26:85–94.

685 27. Sweetser S, Smyrk TC, Sinicrope FA. Serrated colon polyps as precursors to colorectal
686 cancer. Clinical Gastroenterology and Hepatology. 2013;11:760–7.

687 28. Rashtak S, Rego R, Sweetser SR, Sinicrope FA. Sessile serrated polyps and colon cancer
688 prevention. Cancer Prevention Research. 2017;10:270–8.

689 29. Callahan BJ, McMurdie PJ, Rosen MJ, Han AW, Johnson AJA, Holmes SP. DADA2: High-
690 resolution sample inference from Illumina amplicon data. Nat Methods. 2016;13:581–3.

691 doi:10.1038/nmeth.3869.

692 30. Wang Q, Garrity GM, Tiedje JM, Cole JR. Naive Bayesian classifier for rapid assignment of
693 rRNA sequences into the new bacterial taxonomy. Appl Environ Microbiol. 2007;73:5261–7.
694 doi:10.1128/AEM.00062-07.

695 31. Quast C, Pruesse E, Yilmaz P, Gerken J, Schweer T, Yarza P, et al. The SILVA ribosomal
696 RNA gene database project: improved data processing and web-based tools. Nucleic Acids Res.
697 2013;41 Database issue:D590-6. doi:10.1093/nar/gks1219.

698 32. Kopylova E, Noé L, Touzet H. SortMeRNA: Fast and accurate filtering of ribosomal RNAs
699 in metatranscriptomic data. Bioinformatics. 2012;28:3211–7.

700 33. Nawrocki EP, Eddy SR. Infernal 1.1: 100-fold faster RNA homology searches.
701 Bioinformatics. 2013;29:2933–5. doi:10.1093/bioinformatics/btt509.

702 34. Price MN, Dehal PS, Arkin AP. FastTree 2 -- Approximately Maximum-Likelihood Trees
703 for Large Alignments. PLoS One. 2010;5:e9490. doi:10.1371/journal.pone.0009490.

704 35. Lozupone C, Knight R. UniFrac: a New Phylogenetic Method for Comparing Microbial
705 Communities. Appl Environ Microbiol. 2005;71:8228–35.

706 36. McMurdie PJ, Holmes S. phyloseq: An R Package for Reproducible Interactive Analysis and
707 Graphics of Microbiome Census Data. PLoS One. 2013;8:e61217.
708 doi:10.1371/journal.pone.0061217.

709 37. Oksanen J, Kindt R, Legendre P, O'Hara B, Simpson GL, Solymos PM, et al. The vegan
710 package. Community Ecol Packag. 2008;:190.

711 38. Bolker BM, Brooks ME, Clark CJ, Geange SW, Poulsen JR, Stevens MHH, et al.

712 Generalized linear mixed models: a practical guide for ecology and evolution. Trends Ecol Evol.
713 2009;24:127–35.

714 39. Brooks ME, Kristensen K, van Benthem KJ, Magnusson A, Berg CW, Nielsen A, et al.
715 glmmTMB balances speed and flexibility among packages for zero-inflated generalized linear
716 mixed modeling. R J. 2017;9:378–400.

717 40. Orth JD, Thiele I, Palsson BØ. What is flux balance analysis? Nat Biotechnol. 2010;28:245–
718 8. doi:10.1038/nbt.1614.

719 41. Mendes-Soares H, Mundy M, Soares LM, Chia N. MMinte: an application for predicting
720 metabolic interactions among the microbial species in a community. BMC Bioinformatics.
721 2016;17:343.

722 42. Sung J, Kim S, Cabatbat JJT, Jang S, Jin Y-S, Jung GY, et al. Global metabolic interaction
723 network of the human gut microbiota for context-specific community-scale analysis. Nat
724 Commun. 2017;8:15393.

725 43. Shannon P, Markiel A, Ozier O, Baliga NS, Wang JT, Ramage D, et al. Cytoscape: A
726 software Environment for integrated models of biomolecular interaction networks. Genome Res.
727 2003;13:2498–504.

728 44. Wattam AR, Abraham D, Dalay O, Disz TL, Driscoll T, Gabbard JL, et al. PATRIC, the
729 bacterial bioinformatics database and analysis resource. Nucleic Acids Res. 2014;42:D581–91.
730 doi:10.1093/nar/gkt1099.

731 45. Anand S, Kaur H, Mande SS. Comparative In silico Analysis of Butyrate Production
732 Pathways in Gut Commensals and Pathogens. Front Microbiol. 2016;7:1945.

733 doi:10.3389/fmicb.2016.01945.

734 46. Chung L, Thiele Orberg E, Geis AL, Chan JL, Fu K, DeStefano Shields CE, et al.
735 Bacteroides fragilis Toxin Coordinates a Pro-carcinogenic Inflammatory Cascade via Targeting
736 of Colonic Epithelial Cells. Cell Host Microbe. 2018;23:203–214.e5.

737 47. Koi M, Okita Y, M. Carethers J. Fusobacterium nucleatum Infection in Colorectal Cancer:
738 Linking Inflammation, DNA Mismatch Repair and Genetic and Epigenetic Alterations. J Anus,
739 Rectum Colon. 2018;2:37–46.

740 48. Kostic AD, Gevers D, Pedamallu CS, Michaud M, Duke F, Earl AM, et al. Genomic analysis
741 identifies association of Fusobacterium with colorectal carcinoma. Genome Res. 2012;22:292–8.
742 doi:10.1101/gr.126573.111.

743 49. Abed J, Emgård JEM, Zamir G, Faroja M, Almogy G, Grenov A, et al. Fap2 Mediates
744 Fusobacterium nucleatum Colorectal Adenocarcinoma Enrichment by Binding to Tumor-
745 Expressed Gal-GalNAc. Cell Host Microbe. 2016;20:215–25. doi:10.1016/j.chom.2016.07.006.

746 50. Dejea CM, Fathi P, Craig JM, Boleij A, Taddese R, Geis AL, et al. Patients with familial
747 adenomatous polyposis harbor colonic biofilms containing tumorigenic bacteria. Science (80-).
748 2018;359:592–7. doi:10.1126/science.aah3648.

749 51. Coyte KZ, Schluter J, Foster KR. The ecology of the microbiome: Networks, competition,
750 and stability. Science (80-). 2015;350:663–6. doi:10.1126/science.aad2602.

751 52. Eschbach M, Schreiber K, Trunk K, Buer J, Jahn D, Schobert M. Long-term anaerobic
752 survival of the opportunistic pathogen Pseudomonas aeruginosa via pyruvate fermentation. J
753 Bacteriol. 2004;186:4596–604.

754 53. Rivière A, Selak M, Lantin D, Leroy F, De Vuyst L. Bifidobacteria and butyrate-producing
755 colon bacteria: Importance and strategies for their stimulation in the human gut. Frontiers in
756 Microbiology. 2016;7 JUN.

757 54. Pryde SE, Duncan SH, Hold GL, Stewart CS, Flint HJ. The microbiology of butyrate
758 formation in the human colon. FEMS Microbiology Letters. 2002;217:133–9.

759 55. Sousa CP. The versatile strategies of Escherichia coli pathotypes: a mini review. Rev Lit Arts
760 Am. 2006;12:363–73.

761 56. Ulbrich K, Reichardt N, Braune A, Kroh LW, Blaut M, Rohn S. The microbial degradation
762 of onion flavonol glucosides and their roasting products by the human gut bacteria *Eubacterium*
763 *ramulus* and *Flavonifractor plautii*. Food Res Int. 2015;67:349–55.

764 57. Louis P, Flint HJ. Formation of propionate and butyrate by the human colonic microbiota.
765 Environmental Microbiology. 2017;19:29–41.

766 58. Jia F. Genome Sequence of the Oral Probiotic *Streptococcus salivarius* JF. Genome
767 Announc. 2016;4:e00971-16.

768 59. Van Den Abbeele P, Belzer C, Goossens M, Kleerebezem M, De Vos WM, Thas O, et al.
769 Butyrate-producing Clostridium cluster XIVa species specifically colonize mucins in an in vitro
770 gut model. ISME J. 2013;7:949–61.

771 60. Imachi H, Sekiguchi Y, Kamagata Y, Hanada S, Ohashi A, Harada H. Pelotomaculum
772 thermopropionicum gen. nov., sp. nov., an anaerobic, thermophilic, syntrophic propionate-
773 oxidizing bacterium. Int J Syst Evol Microbiol. 2002;52:1729–35.

774 61. Dehoux P, Marvaud JC, Abouelleil A, Earl AM, Lambert T, Dauga C. Comparative

775 genomics of Clostridium bolteae and Clostridium clostridioforme reveals species-specific
776 genomic properties and numerous putative antibiotic resistance determinants. BMC Genomics.
777 2016;17.

778 62. Kageyama A, Benno Y. Coprobacillus catenaformis gen. nov., sp. nov., a new genus and
779 species isolated from human feces. Microbiol Immunol. 2000;44:23–8.

780 63. Wannemuehler MJ, Overstreet A, Ward D V, Phillips GJ. Draft genome sequences of the
781 altered schaedler flora, a defined bacterial community from gnotobiotic mice. Genome Announc.
782 2014;2:1–2.

783 64. Jeraldo P, Hernández Á, White BA, O'Brien D, Ahlquist D, Boardman L, et al. Draft
784 Genome Sequences of 24 Microbial Strains Assembled from Direct Sequencing from 4 Stool
785 Samples. Genome Announc. 2015;3:e00526-15. doi:10.1128/genomeA.00526-15.

786 65. Tatusova T, Ciufo S, Fedorov B, O'Neill K, Tolstoy I. RefSeq microbial genomes database:
787 new representation and annotation strategy (vol 42, pg 553, 2014). Nucleic Acids Res.
788 2015;43:3872.

789 66. Han YW. Fusobacterium nucleatum: A commensal-turned pathogen. Current Opinion in
790 Microbiology. 2015.

791 67. Lawson PA, Song Y, Liu C, Molitoris DR, Vaisanen ML, Collins MD, et al. Anaerotruncus
792 colihominis gen. nov., sp. nov., from human faeces. Int J Syst Evol Microbiol. 2004;54:413–7.

793 68. Louis P, Flint HJ. Diversity, metabolism and microbial ecology of butyrate-producing
794 bacteria from the human large intestine. FEMS Microbiol Lett. 2009;294:1–8.

795 69. Shinha T. Fatal Bacteremia Caused by Campylobacter gracilis, United States. Emerg Infect

796 Dis. 2015;21:1084–5. doi:10.3201/eid2106.142043.

797 70. Attene-Ramos MS, Nava GM, Muellner MG, Wagner ED, Plewa MJ, Gaskins HR. DNA
798 damage and toxicogenomic analyses of hydrogen sulfide in human intestinal epithelial FHs 74
799 int cells. Environ Mol Mutagen. 2010;51:304–14.

800 71. Wolf PG, Parthasarathy G, Chen J, O'Connor HM, Chia N, Bharucha AE, et al. Assessing
801 the colonic microbiome, hydrogenogenic and hydrogenotrophic genes, transit and breath
802 methane in constipation. Neurogastroenterol Motil. 2017.

803 72. Lee ZW, Zhou J, Chen CS, Zhao Y, Tan CH, Li L, et al. The slow-releasing Hydrogen
804 Sulfide donor, GYY4137, exhibits novel anti-cancer effects in vitro and in vivo. PLoS One.
805 2011;6.

806 73. Hellmich MR, Coletta C, Chao C, Szabo C. The Therapeutic Potential of Cystathionine β-
807 Synthetase/Hydrogen Sulfide Inhibition in Cancer. Antioxid Redox Signal. 2015;22:424–48.

808 74. Richman S. Deficient mismatch repair: Read all about it (Review). International Journal of
809 Oncology. 2015;47:1189–202.

810 75. Cai W, Wang M, Ju L, Wang C, Zhu Y. Hydrogen sulfide induces human colon cancer cell
811 proliferation: role of Akt, ERK and p21. Cell Biol Int. 2010;34:565–72.

812 76. Purcell R V., Pearson J, Aitchison A, Dixon L, Frizelle FA, Keenan JI. Colonization with
813 enterotoxigenic Bacteroides fragilis is associated with early-stage colorectal neoplasia. PLoS
814 One. 2017;12.

815 77. Maiuri AR, Peng M, Sriramkumar S, Kamplain CM, DeStefano Shields CE, Sears CL, et al.
816 Mismatch repair proteins initiate epigenetic alterations during inflammation-driven

817 tumorigenesis. Cancer Res. 2017;77:3467–78.

818 78. Lupton JR. Microbial degradation products influence colon cancer risk: the butyrate
819 controversy. J Nutr. 2004;134:479–82.

820 79. Magnúsdóttir S, Thiele I. Modeling metabolism of the human gut microbiome. Current
821 Opinion in Biotechnology. 2018;51:90–6.

822 80. Benedict MN, Mundy MB, Henry CS, Chia N, Price ND. Likelihood-Based Gene
823 Annotations for Gap Filling and Quality Assessment in Genome-Scale Metabolic Models. PLoS
824 Comput Biol. 2014;10:e1003882. doi:10.1371/journal.pcbi.1003882.

825 81. Magnúsdóttir S, Heinken A, Kutt L, Ravcheev DA, Bauer E, Noronha A, et al. Generation of
826 genome-scale metabolic reconstructions for 773 members of the human gut microbiota. Nat
827 Biotechnol. 2016. doi:10.1038/nbt.3703.

828

829

Additional File 1

Figure S1: Venn diagram highlighting number of microbes that overlap between tumor and normal samples in relation to MMR status (dMMR = red font, pMMR = green font, red circles = tumor samples, blue circles = normal samples). Only differentially abundant microbes with a corrected p-value < 0.05 were included in this diagram.

Figure S2: Differentially abundant OTUs between patient–matched tumor and normal samples in individuals with dMMR CRC. Y-axis indicates percent relative abundance of OTUs. Line color indicates directionality of change in microbial abundance: red = increased abundance relative to normal, blue = decreased abundance or no change compared to normal.

Table S1. Factors contributing to variance between microbial communities. Sample location was included as the last variable in this model (PERMANOVA).

Table S2. Factors contributing to variance between microbial communities. Sample location was included as the last variable in this model (PERMANOVA).

Table S3: sOTUs enriched in tumor samples (colon tissue and mucosa) as compared to normal–adjacent samples in individuals with dMMR CRC.

Table S4: sOTUs enriched in tumor samples (colon tissue and mucosa) as compared to normal–adjacent samples in individuals with pMMR CRC.

Table S5: Differentially abundant microbes in individuals with dMMR CRC. Blue boxes highlight microbes enriched in tumor tissue samples as compared to normal–adjacent samples.

Table S6: Differentially abundant microbes in individuals with pMMR CRC. Blue boxes highlight microbes enriched in tumor tissue samples as compared to normal–adjacent samples.

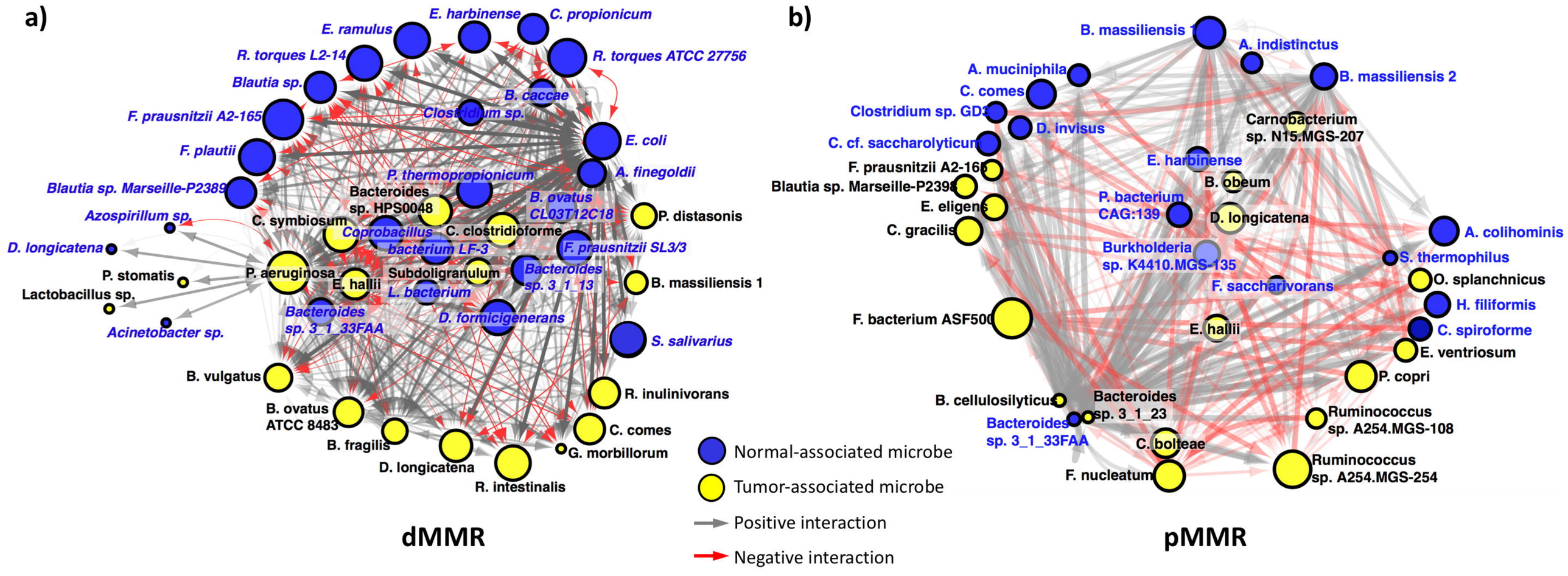
a)
E. harbinense
C. propionicum
E. ramulus
R. torques L2-14
R. torques ATCC 27756
Blautia sp.
B. caccae
F. prausnitzii A2-165
Clostridium sp.
E. coli
F. plautii
A. finegoldii
Blautia sp. Marseille-P2389
P. thermopropionicum
Bacteroides
sp. HPS0048
B. ovatus
CL03T12C18
P. distasonis
Azospirillum sp.
C. symbiosum
Coprobacillus
C. clostridioforme
D. longicatena
bacterium LF-3
F. prausnitzii SL3/3
P. stomatis
P. aeruginosa
E. hallii
Subdoligranulum
Bacteroides
sp. 3_1_13
B. massiliensis 1
Lactobacillus sp.
L. bacterium
Bacteroides
sp. 3_1_33FAA
D. formicigenerans
Acinetobacter sp.
S. salivarius
B. vulgatus
R. inulinivorans
B. ovatus
ATCC 8483
C. comes
B. fragilis
G. morbillorum
D. longicatena
R. intestinalis
dMMR
b)
B. massiliensis 1
A. indistinctus
A. muciniphila
B. massiliensis 2
C. comes
Clostridium sp. GD3
D. invisus
Carnobacterium
sp. N15.MGS-207
C. cf. saccharolyticum
E. harbinense
F. prausnitzii A2-165
B. obeum
Blautia sp. Marseille-P2398
P. bacterium
CAG:139
E. eligens
D. longicatena
C. gracilis
A. colihominis
Burkholderia
sp. K4410.MGS-135
S. thermophilus
F. saccharivorans
O. splanchnicus
H. filiformis
F. bacterium ASF500
E. hallii
C. spiroforme
E. ventriosum
P. copri
B. cellulosilyticus
Bacteroides
sp. 3_1_23
Ruminococcus
sp. A254.MGS-108
Bacteroides
sp. 3_1_33FAA
C. bolteae
Ruminococcus
sp. A254.MGS-254
F. nucleatum
pMMR
Normal-associated microbe
Tumor-associated microbe
Positive interaction
Negative interaction

dMMR Tumor	dMMR Normal
Bacteroides fragilis YCH46 *Fusobacterium periodonticum 2_1_31* *Fusobacterium nucleatum CTI-5** *Roseburia intestinalis M50/1** *Bacteroides sp. HPS0048* *Peptostreptococcus stomatis DSM 17678* *Clostridium clostridioforme 90A1* *[Clostridium] symbiosum* *Pseudomonas aeruginosa strain NCTC10332* ***Coprococcus comes ATCC 27758*** *Eggerthella lenta DSM 2243* *Roseburia inulinivorans** ***Bacteroides massiliensis B84634*** *Bacteroides vulgatus ATCC 8482* *Parabacteroides distasonis ATCC 8503* ***Dorea longicatena*** *Lactobacillus sp. N15.MGS-260* *Bacteroides ovatus strain ATCC 8483* *Subdoligranulum sp. 4_3_54A2FAA** *[Eubacterium] hallii** *major butyrate producers	*Bacteroides sp. 3_1_33FAA* *Escherichia coli str. K-12 substr. MG1655* *Ruminococcus torques ATCC 27756** *Bacteroides vulgatus ATCC 8482* *Bacteroides ovatus CL03T12C18* *Faecalibacterium prausnitzii SL3/3** ***Faecalibacterium prausnitzii A2-165**** *Bacteroides sp. 3_1_13* *Clostridium sp. JCC* *Alistipes finegoldii* *Lachnospiraceae bacterium mt14** *bacterium LF-3* ***Blautia sp. Marseille-P2398**** *Coprobacillus sp. 8_1_38FAA* *Ruminococcus torques L2-14** *Eubacterium ramulus* *Dorea longicatena DSM 13814* *Streptococcus salivarius strain JF* ***Ethanoligenens harbinense YUAN-3*** *Bacteroides caccae CL03T12C61* *Azospirillum sp. CAG:260* *Dorea formicigenerans ATCC 27755* *Pelotomaculum thermopropionicum SI* *Acinetobacter sp. N54.MGS-139* *[Clostridium] propionicum DSM 1682*
pMMR Tumor	**pMMR Normal**
Prevotella copri DSM 18205 *Ruminococcus sp. A254.MGS-108** *Odoribacter splanchnicus DSM 220712** *Campylobacter gracilis strain ATCC 33236* *Bacteroides cellulosilyticus strain WH2* *Bacteroides sp. 3_1_23* *Firmicutes bacterium ASF500** *Clostridium bolteae 90A9** ***Blautia sp. Marseille-P2398**** ***Dorea longicatena*** ***Faecalibacterium prausnitzii A2-165**** *Ruminococcus sp. A254.MGS-254**	***Bacteroides massiliensis B84634*** ***Ethanoligenens harbinense YUAN-3*** ***Coprococcus comes ATCC 27758*** *Dialister invisus DSM 15470* *Proteobacteria bacterium CAG:139* *Clostridium cf. saccharolyticum K10** *Fusicatenibacter saccharivorans* *Holdemania filiformis DSM 12042* *Burkholderia sp. K4410.MGS-135*

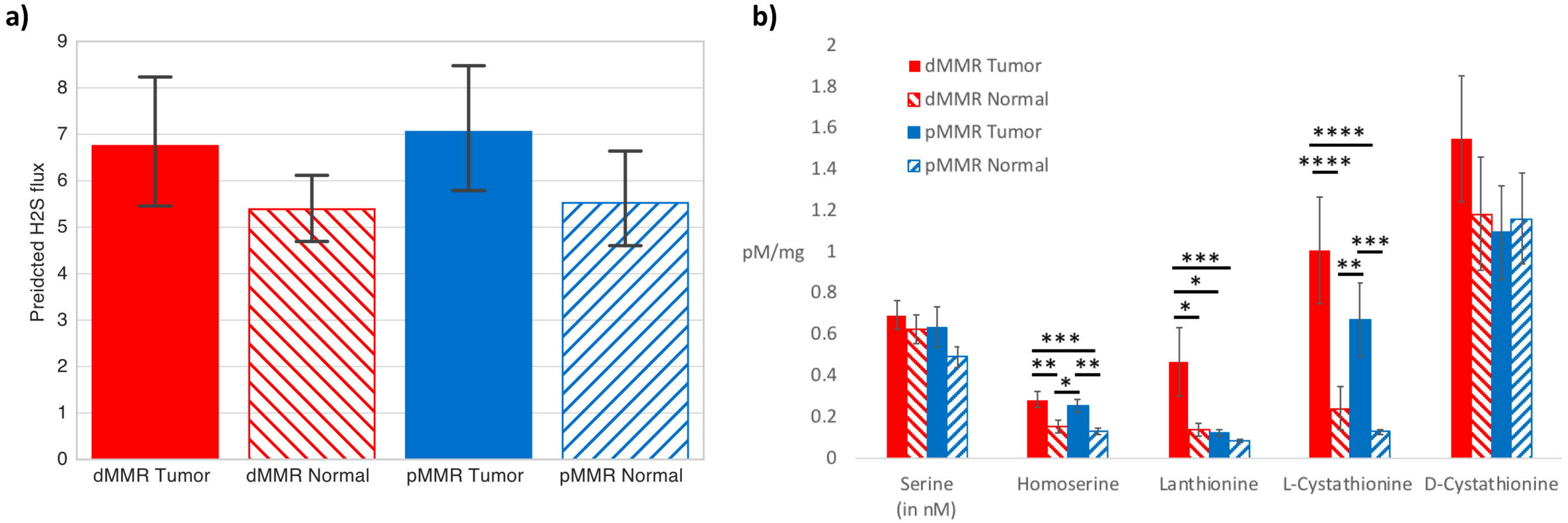
a)
Preidcted H2S flux
0
1
2
3
4
5
6
7
8
9
dMMR Tumor
dMMR Normal
pMMR Tumor
pMMR Normal
b)
pM/mg
0
0.2
0.4
0.6
0.8
1
1.2
1.4
1.6
1.8
2
dMMR Tumor
dMMR Normal
pMMR Tumor
pMMR Normal
Serine (in nM)
Homoserine
Lanthionine
L-Cystathionine
D-Cystathionine
*
**
***
****